International Journal of Mass Spectrometry 306 (2011) 123–128

Contents lists available at ScienceDirect

International Journal of Mass Spectrometry

journal homepage: www.elsevier.com/locate/ijms

Electron attachment to $POCl_3$. II. Dependence of the attachment rate coefficients on gas and electron temperature

Nicholas S. Shuman[a], Thomas M. Miller[a], Albert A. Viggiano[a], Jürgen Troe[b,c,*]

[a] Air Force Research Laboratory, Space Vehicles Directorate, Hanscom Air Force Base, Bedford, MA 01731-3010, USA
[b] Institut für Physikalische Chemie, Universität Göttingen, Tammannstrasse 6, D-37077 Göttingen, Germany
[c] Max-Planck-Institut für biophysikalische Chemie, Am Fassberg 11, D-37077 Göttingen, Germany

ARTICLE INFO

Article history:
Received 31 August 2010
Accepted 28 September 2010
Available online 8 October 2010

Keyword:
Electron attachment

ABSTRACT

Rate coefficients for attachment of electrons to $POCl_3$ have been measured in two FALP (flowing-afterglow Langmuir-probe) apparatuses, extending the temperature range of earlier experiments. The results for equal gas and electron temperatures are compared with data for independently varied temperatures. An analysis of the rate coefficients in terms of electron-polar target capture theory leads to empirical electron–phonon coupling factors which are markedly smaller than unity. These factors depend on the electron energy but do not seem to depend on the gas temperature, which is in contrast to observations made for the electron attachment to SF_6. Besides s-wave attachment, contributions from higher partial waves are analyzed and suggested to contribute to some extent. Attachment cross sections and specific rate constants for electron autodetachment are finally constructed in a way which is consistent with the experimental attachment rate coefficients. Autodetachment is shown to be negligible compared to dissociation of $POCl_3^-$ which is analyzed in a subsequent publication.

1. Introduction

Electron attachment rate coefficients k_{at} are known to depend on the temperature of the electrons, T_{el}, and of the neutral target species, T_{gas}, in an intricate way, see e.g. Ref. [1]. There are a number of factors which contribute to the experimental k_{at} (T_{el}, T_{gas}). An upper limit to k_{at} is provided by the rate coefficient k_{cap} (T_{el}) for capture of the electron by the target molecule (polar with dipole moment μ_D and/or polarizable with polarizability α). k_{cap} can be calculated from generalized Vogt–Wannier capture theory, see Refs. [2–6]. Whether the captured electron finally is "integrated" into the electronic shell of the neutral target forming an anionic state, depends on the efficiency of the coupling between electron and target nuclear motions, i.e. on "electron–phonon coupling" or "intramolecular vibrational redistribution (IVR)". If metastable anions are formed by IVR, they may subsequently redetach the electron, dissociate, or be stabilized by collisions or radiation which may introduce a bath gas pressure dependence [7] in addition to the dependences on T_{el} and T_{gas}.

In order to rationalize the analysis of experimental attachment rate coefficients k_{at}, in Ref. [7] we have analyzed the role of secondary processes by kinetic modelling. Provided that k_{at} corresponds to the primary attachment process only, such as we shall assume in the present article, we compare the experimental k_{at} with calculated capture rate coefficients, k_{cap}, and we represent the difference by IVR factors, P^{IVR}, to be defined either on the level of attachment rate coefficients or cross sections, see below. Further interpretation of the empirically derived IVR factors may be done by rigorous theory or by empirical considerations.

We express the dependence of the IVR factors on the electron temperature T_{el} by the dependence on a reduced temperature θ defined by:

$$\theta = \left(\frac{e\mu}{\hbar^2}\right)\alpha k T_{el} \tag{1.1}$$

Likewise, we express the dependence on the electron energy E_{el} through a reduced wave vector κ defined by:

$$\kappa = \frac{\mu e(2\alpha E_{el})^{1/2}}{\hbar^2} \tag{1.2}$$

We hence consider IVR factors in the attachment rate coefficients,

$$k_{at}(T_{el},\ T_{gas}) = P_k^{IVR}(\theta,\ T_{gas})k_{cap}(\theta) \tag{1.3}$$

or in the attachment cross sections,

$$\sigma_{at}(\kappa,\ T_{gas}) = P_\sigma^{IVR}(\kappa,\ T_{gas})\sigma_{cap}(\kappa) \tag{1.4}$$

Instead of the dependence on the bath gas temperature T_{gas}, more generally a dependence on individual rovibrational states of the neutral target molecule could be specified.

* Corresponding author. Tel.: +49 551 39 3121; fax: +49 49 551 39 3150.
E-mail addresses: afrl.rvb.pa@hanscom.af.mil (A.A. Viggiano), shoff@gwdg.de (J. Troe).

1387-3806/$ – see front matter © 2010 Elsevier B.V. All rights reserved.
doi:10.1016/j.ijms.2010.09.026

An important contribution to the P^{IVR} are Franck–Condon factors for overlap of the nuclear wave functions of the neutral and anion potential energy surfaces, differing for endothermic or exothermic cases, with or without intermediate barriers along the nuclear coordinates [1]. Obviously, these contributions vary with the vibrational state of the neutral target and depend on T_{gas}. Generally there will be an additional electron–phonon coupling contribution which, within a given vibrational state of the target, depends on the electron energy E_{el} and the partial wave of the electron. In favourable cases, this can be characterized by resonance R-matrix theory [8] which, however, generally requires empirical adjustment of some fit parameters. On a more operational level, we suggested [7] to directly characterize empirical P^{IVR} such as derived by comparing the experimental $k_{at}(T_{el}, T_{gas})$ with the calculated $k_{cap}(T_{el})$.

Our first example treated in this way [7] was the electron attachment to SF_6 where P_σ^{IVR} was tentatively expressed in the form

$$P^{IVR}(\kappa,\ T_{gas}) = \exp[-c_1\kappa^2] \tag{1.5}$$

with a fit parameter c_1 which empirically was found to decrease with increasing T_{gas}. $k_{cap}(T_{el})$ in this system was assumed to be dominated by s-wave capture. An analogous analysis was made [9] for electron attachment to SF_5Cl. Here, an additional preexponential factor $A(T_{gas})$ being smaller than unity was required to fit k_{at} and σ_{at} at the same time, i.e.

$$P^{IVR}(\kappa,\ T_{gas}) = A(T_{gas})\exp[-c_1\kappa^2] \tag{1.6}$$

was chosen. The factor $A(T_{gas})$ was suggested to account for a Franck–Condon overlap which was less complete than for the SF_6 system.

Separating the dependences of k_{at} on T_{gas} and T_{el} (or E_{el}) requires a considerable amount of experimental work. This has been performed for electron attachment to SF_6, see Refs. [7,9] and the work cited therein. Looking for systems with similarly detailed experimental information, one may consider the electron attachment to $POCl_3$. In part I of this work [10], for this system k_{at} was measured over the range 297–552 K of T_{gas} and 297–6800 K of T_{el}. At the same time, branching fractions were measured as functions of bath gas pressure for $T_{gas} = T_{el}$. New measurements of branching fractions over an extended temperature range and their detailed analysis will be described in part III of this series [11] and are not subject of the present article. Here we extend measurements of primary attachment rate coefficients k_{at} beyond the results of part I [10] and earlier work [12], and we perform a more detailed analysis of the dependence of k_{at} on T_{el} and T_{gas} than this was possible in part I. The comparison with the SF_6-system appears particularly attractive because $POCl_3$, in contrast to SF_6, has a permanent dipole moment affecting k_{cap}. As high electron temperatures were studied, it also appeared interesting to investigate whether there are indications for contributions from higher than s-partial waves of the electrons.

2. Experimental rate coefficients for attachment

2.1. Experimental apparatus

Two flowing-afterglow Langmuir-probe (FALP) apparatuses were used in measuring k_{at} for $POCl_3$. One was the conventional FALP apparatus (300–550 K) which has been described in detail in Refs. [13,14]. The second was a high-temperature FALP apparatus (HT-FALP, 300–1200 K), which has also been described in the literature [15], as has the FALP method itself [16]. A few details are given in the following. In both the apparatuses, a microwave discharge is used to establish a weak plasma in a fast flow of He buffer gas (with about 2% Ar added downstream) in a cylindrical flow tube (about 7 cm diameter, about 1 m length) at pressures typically of 1–2 Torr. The electron-Ar^+ (containing some He^+) plasma concentration decays down the length of the flow tube by ambipolar diffusion. If an electron-attaching gas (e.g., $POCl_3$) is added through an inlet located approximately halfway downstream in the flow tube, the plasma concentration decays faster beyond that point, depending on the attachment rate coefficient and concentration of the gas. A movable Langmuir probe was used to measure the electron concentration along the flow tube axis [15]. The probe was also used to determine the propagation time of a pulse disturbance of the plasma, to provide a time scale for the measurements made along the length of the flow tube. If diffusion were a negligible loss mechanism for the plasma, electron attachment would result in a simple exponential decay of the electron concentration. The reality is that the electron concentration $n_e(t)$ decays in time t according to the coupled effects of diffusion and attachment [16,17],

$$n_e(t) = \frac{n_e(0)[\upsilon_a \exp(-\upsilon_a t) - \upsilon_D \exp(-\upsilon_D t)]}{(\upsilon_a - \upsilon_D)} \tag{2.1}$$

where $n_e(0)$ is the electron concentration at the reactant gas inlet ($t = 0$), and υ_a is the electron attachment rate, related to the attachment rate constant k_{at} and the reactant concentration n_r by $\upsilon_a = k_{at} n_r$ [5–7]. The diffusion rate, υ_D, is measured in absence of reactant gas. At the downstream end of the flow tube ions are sampled through a small aperture (330 μm diameter) for mass analysis and detection. Ion-molecule reaction studies are carried out to determine mass discrimination correction factors [18]. Neutral products of reactions are not observed in these experiments.

The FALP and HT-FALP apparatuses have engineering differences related to the fact that the main part of the HT-FALP flow tube is enclosed in a commercial furnace, so that all ports must enter the flow tube from the upstream end (i.e., Langmuir probe, gas inlet tubes, pressure measurement tube, and thermocouple temperature sensor) [15]. The HT-FALP utilizes a quartz flow tube, while the FALP flow tube is stainless steel. The HT-FALP mass spectra show background ions, positive and negative, due to imperfect sealing of the quartz flow tube against the vacuum box containing the furnace. In the FALP, the plasma is maintained at ground potential by the stainless steel flow tube. In the HT-FALP, ground potential is established by a stainless steel tee through which the plasma flows on its way to the main (heated) quartz flow tube. Above 900 K, the Langmuir probe current-voltage characteristic (HT-FALP) shows distortion on the negatively-biased side which we believe is related to thermionic emission, but does not appear to affect the electron concentration measurement on the positively-biased side [15]. Plasma velocity measurements are straightforward at low temperatures in both apparatuses, but the pulses undergo greater diffusion in the HT-FALP at high temperatures. Because of this, plasma velocities at temperatures >500 K in the HT-FALP were calculated from the buffer gas bulk velocity by multiplying by a factor 1.7 as determined from measurements at lower temperatures. The bulk velocity was obtained from the buffer gas volume flow rate (measured with MKS Instruments flowmeters) divided by the cross sectional area of the flow tube. As is well known, the plasma velocity is faster than the bulk gas flow velocity because the plasma radial profile overlaps more of the faster-moving part of the parabolic velocity profile of the buffer gas in laminar flow [15]. Aside from these differences, the FALP and HT-FALP apparatuses use different gas flowmeters and pressure-measuring instruments, which has the potential to result in several percent differences in measured diffusion and attachment rate coefficients. The main uncertainty in the k_{at} measurements is in knowing the concentration of reactant ($POCl_3$) in the flow tube. This concentration (typically 3 parts per million in the buffer gas) is determined from measurement of the total gas pressure and the volume flow rates of buffer and reactant gases. The uncertainty in measurements of $n_e(t)$ using the Langmuir probe are not directly involved, aside from the importance of linearity, because it is only the change in $n_e(t)$ that matters, as long

Table 1
Experimental rate coefficients for electron attachment to $POCl_3$ vs temperature ($T_{gas} = T_{el}$), (measurements on the FALP and HT-FALP apparatuses).

T_{gas}/K	k_{at}(FALP)/cm^3 s^{-1}	k_{at}(HT-FALP)/cm^3 s^{-1}
300	1.8×10^{-7}	1.8×10^{-7}
400	1.4×10^{-7}	–
500	1.2×10^{-7}	–
503	–	1.5×10^{-7}
602	–	1.1×10^{-7}
697	–	7.6×10^{-8}
805	–	6.5×10^{-8}
853	–	6.5×10^{-8}
900	–	5.5×10^{-8}
957	–	6.4×10^{-8}
1031	–	6.6×10^{-8}
1110	–	5.0×10^{-8}
1200	–	6.3×10^{-8}
1210	–	4.8×10^{-8}

as $n_e(t)$ is small enough that electron–cation and ion–ion neutralization reactions are negligible. Overall, we estimate the average k_{at} in this work to be accurate to ±25%.

2.2. Experimental rate coefficients

Experimental k_{at} measured with the FALP and HT-FALP apparatuses for $POCl_3$ are presented in Table 1. We have previously published k_{at} using the FALP apparatus with $POCl_3$, 296–552 K [12]. A later FALP study in which the electron temperature T_e was varied yielded a higher value for the room temperature k_{at}, though within uncertainties [10]. In the present work we have tried to pin down the room temperature value of $k_{at}(POCl_3)$ through comparison with $k_{at}(SF_6)$, which is accurately known ($2.27 \pm 0.7 \times 10^{-7}$ cm^3 s^{-1}) and comparable in magnitude to $k_{at}(POCl_3)$ [19]. The present room temperature results agree with the lower values of k_{at} determined in the original study. There is a small discrepancy between the current FALP and HT-FALP rate constants at 500 K. We have been unable to determine the cause of the discrepancy, and using an average of the FALP and HT-FALP results is the best that can be done at present. The attachment reaction is interesting partly because the nascent $POCl_3^-$ anion can either be stabilized or dissociates. New measurements of the branching fractions and modelling of the unimolecular processes will be presented in paper III of this series [11].

3. Calculation of rate coefficients and cross sections for electron capture by $POCl_3$

The experimental attachment rate coefficients k_{at} of Section 2 are compared with calculated capture rate coefficients k_{cap} in this section. In order to obtain information on the contribution from higher partial waves of the electrons relative to that of s-wave electrons, we compare s-wave and higher-wave capture rate coefficients. We base our analysis on the results of Refs. [4,20]. The molecular parameters of $POCl_3$ used in the calculations are the polarizability, $\alpha = 10.06 \times 10^{-24}$ cm^3, and a dipole moment, $\mu_D = 2.54$ (±0.05) D. We are not aware of measurements of α. The above value is from a B3LYP/6-311 + G(3df) DFT calculation, while the empirical additivity method of Ref. [21] gives 9.85×10^{-24} cm^3, i.e. in good agreement. The value for μ_D is from Ref. [22]; our DFT calculation finds 2.42 D. With the given values of α and μ_D, the characteristic parameters of the system are determined, such as the reduced dipole moment

$$d = \frac{e\mu\mu_D}{\hbar^2} = 1.0 \tag{3.1}$$

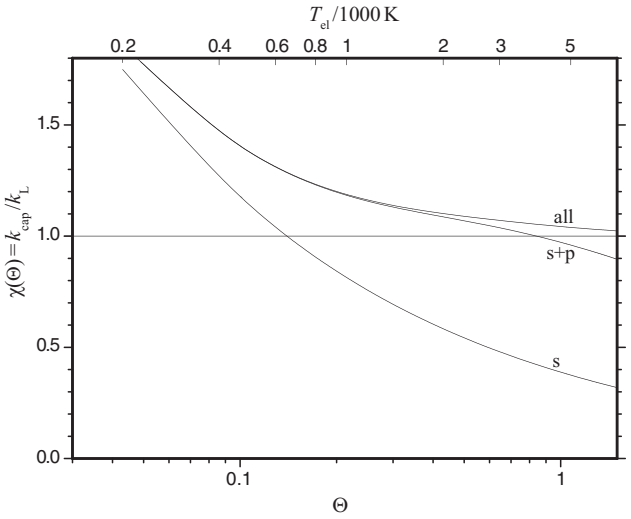

Fig. 1. Reduced rate coefficients $\chi(\theta) = k_{cap}/k_L$ for capture of electrons by $POCl_3$ as a function of the reduced electron temperature θ (lowest curve: s-waves, $l = 0$; middle curve: s- and p-waves, $l = 0$ and 1; upper curve: all-waves $l = 0, 1, 2, \ldots$; see text).

the reduced temperature θ of Eq. (1.1), i.e.

$$\theta = 6.45 \times 10^{-2} \left(\frac{T_{el}}{300\,\text{K}} \right) \tag{3.2}$$

and the Langevin rate constant

$$k_L = 2\pi e \left(\frac{\alpha}{\mu} \right)^{1/2} = 3.17 \times 10^{-7}\,\text{cm}^3\,\text{s}^{-1} \tag{3.3}$$

We express our results in the form of reduced rate coefficients χ defined by:

$$\chi(\theta) = \frac{k_{cap}}{k_L} \tag{3.4}$$

Numerical reduced rate coefficients, for $d = 1$, have been obtained in Ref. [4] for s-wave capture, $\chi_s(\theta)$, as well as for all-wave capture, $\chi(\theta)$, in Ref. [5]. Fig. 1 compares the results. One observes that $\chi_s(\theta)/\chi(\theta) > 0.7$ as long as $\theta < 0.12$ which in the present case corresponds to $T_{el} < 600$ K. On the other hand, $\chi_s(\theta)/\chi(\theta) = 0.3$ at $\theta = 1.2$, corresponding to $T_{el} \approx 6000$ K. Capture rate coefficients k_{cap} according to Fig. 1 are larger than the Langevin rate constant $k_L = 3.17 \times 10^{-7}$ cm^3 s^{-1} over wide temperature ranges. The comparison with the experiments from Ref. [10] shows that $k_{at} < k_{cap}$ which we empirically represent by IVR factors P^{IVR} smaller than unity. Even if an uncertainty of up to a factor of two of the experimental results is allowed for, the experimental data fall to values well below the capture results, i.e. IVR factors markedly below unity are observed. There does not appear to be a dependence of the IVR factors on the gas temperature T_{gas} which is in contrast to what was observed for the SF_6-system in Ref. [7]. Instead, the temperature dependence of the experimental attachment rate coefficients appears to be dominated by the dependence on the electron temperature T_{el}.

The experimental results of $k_{at} = (1.5 - 2) \times 10^{-8}$ cm^3 s^{-1} (corresponding to $\chi = 0.05 - 0.07$) at $T_{el} > 3000$ K (corresponding to $\theta > 0.6$) may suggest a major contribution from higher partial waves, although that would also imply IVR factors markedly smaller than unity. Although there is no way to unambiguously separate the IVR factors for s-wave and higher wave-capture on the basis of Fig. 2, we try to provide a tentative separation in the following. We do this by employing IVR factors for cross sections of the form of Eqs. (1.5)

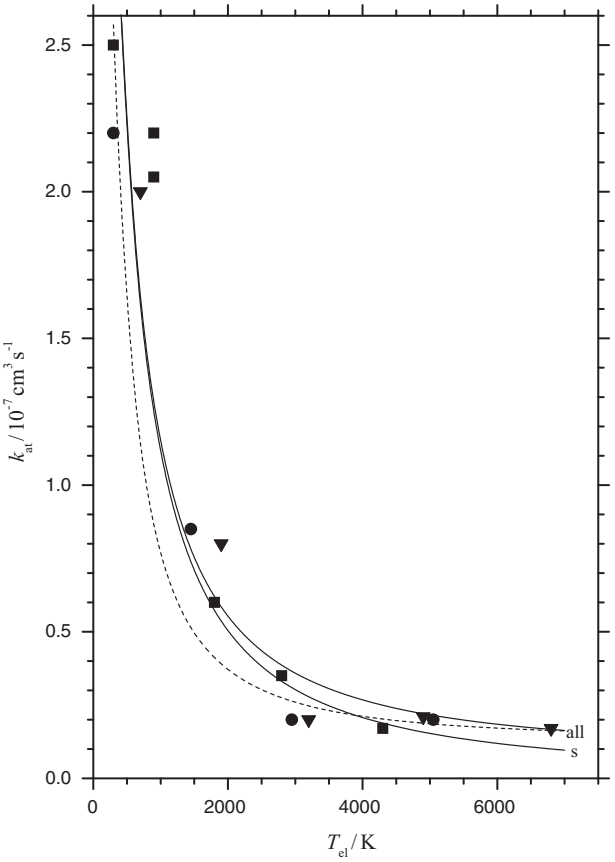

Fig. 2. Rate coefficients k_{at} for attachment of electrons to $POCl_3$ (points = experiments from Ref. [10] at T_{gas} = 305 K (■), 372 K (●), and 552 K (▼); —: fit with IVR parameters (c_1, c_2) = (3, 0.03), upper curve: all-waves, lower curve: s-waves; - - -: fit with IVR parameters (c_1, c_2) = (6, 0.05), all-waves; see text).

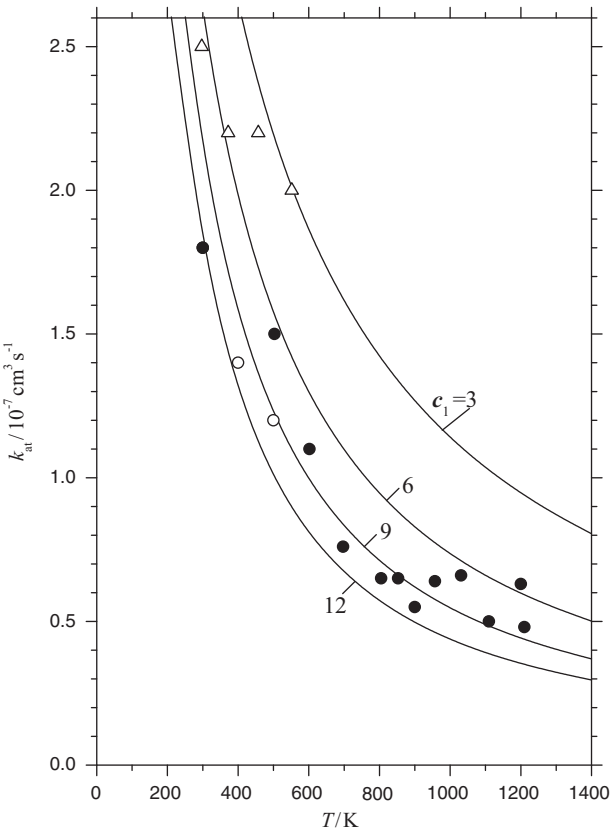

Fig. 3. Rate coefficients k_{at} for attachment of electrons to $POCl_3$ ($T = T_{gas} = T_{el}$; experimental points: △ from Ref. [10], ○ from this work (FALP) and ● from this work (HT-FALP); lines = fit with variable IVR parameter c_1 (c_2 = 0.03), see text).

and (1.6). In this case, cross sections are thermally averaged over a Maxwell–Boltzmann distribution $F(\kappa,\theta)$ which has the form

$$F(\kappa,\,\theta) = 2\kappa^2\theta^{-3/2}(2\pi)^{-1/2}\exp\left(\frac{-\kappa^2}{2\theta}\right) \tag{3.5}$$

where $\kappa = 2.234\,(E_{el}/\mathrm{eV})^{1/2}$ according to Eq. (1.2).With capture cross sections

$$\sigma_{cap}(E_{el}) = \left(\frac{\pi\hbar^2}{2\mu E_{el}}\right)\sum_{l=0}^{\infty}\sum_{m=-l}^{l}P_{l,m}(\kappa) \tag{3.6}$$

all-wave and s-wave reduced capture rate coefficients are obtained as:

$$\chi_{all}(\theta) = \sum_{l=0}^{\infty}\sum_{m=-l}^{l}\int_0^{\infty}(2\kappa)^{-1}P_{l,m}(\kappa)F(\kappa,\theta)\mathrm{d}\kappa \tag{3.7}$$

and

$$\chi_s\left(\theta\right) = \int_0^{\infty}(2\kappa)^{-1}P_s(\kappa)F(\kappa,\theta)\mathrm{d}\kappa \tag{3.8}$$

where the $P_{l,m}(\kappa)$ denote the attachment probabilities. The maximum of these probabilities is provided by the capture probabilities $P_{l,m}^{VW}(\kappa)$ from extended Vogt–Wannier capture theory. For polarizable molecules, they have been calculated in detail and represented in approximate analytical form over the range l = 0–12 in Refs. [4,6]. The corresponding results for targets with permanent dipole moment (i.e. $d > 0$) are given in the form of analytical approximations in a separate publication [20] (data for the present case are given in Appendix A). One should note the large difference between $P_{0,0}^{VW}(\kappa, d) = P_s^{VW}(\kappa, d)$ for nonpolar target molecules (d = 0), i.e.

$$P_s^{VW}(\kappa, d = 0) \approx 1 - 0.25\exp(-1.387\kappa) - 0.75\exp(-4.871\kappa) \tag{3.9}$$

and for polar targets, e.g.:

$$P_s^{VW}(\kappa, d = 1) \geq 0.9 \tag{3.10}$$

for the present case (see Fig. 4 of Ref. [4]; the small κ-dependence of P_s^{VW} (κ,d = 1) between 0.9 and 1 is not very relevant; for more accurate results, see Appendix A).

In order to rationalize the experiments of Fig. 2, we first consider s-wave capture probabilities $P_s(\kappa)$ in the form of

$$P_s(\kappa) = P_s^{IVR}(\kappa)P_s^{VW}(\kappa) \tag{3.11}$$

with $P_s^{VW}(\kappa)$ from Eq. (3.10). We again employ $P_s^{IVR}(\kappa)$ in the tentative form of Eq. (1.5) with a fitting parameter c_1. The experimental data are certainly not sufficiently precise to allow for a separation of s-wave and higher-wave contributions. One may specify the functional form of IVR factors of higher waves with less precision. For simplicity, therefore, we employ an energy-independent $P_{n,m}^{IVR} = c_2$ for $n \geq 1$. Fig. 2 compares two alternative representations of the experimental data from Ref. [10], one with c_1 = 3 and c_2 = 0.03, and one with c_1 = 6 and c_2 = 0.05. For the former, s-wave and all-wave contributions are shown separately.

The experimental uncertainties unfortunately prevent us from a more accurate determination of the fit parameters c_1 and c_2. This is illustrated in Fig. 3 where results from Ref. [10] and the present results from our two FALP systems up to 1200 K, all with $T_{gas} = T_{el}$, are compared with fits varying c_1 between 3 and 12 (keeping c_2 constant at a value of 0.03). The new data are best represented with c_1 = 9 and c_2 = 0.03. For comparison, we note that fit parame-

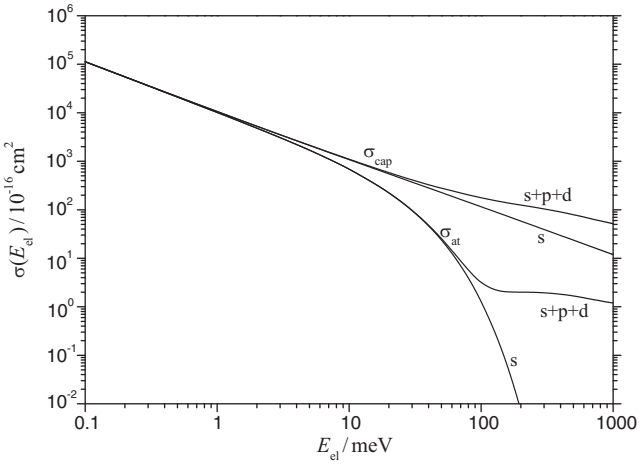

Fig. 4. Cross sections for capture σ_{cap} and attachment σ_{at} of electrons to $POCl_3$ (calculations for s-waves and s + p + d-waves; IVR fit parameters $(c_1, c_2) = (9, 0.03)$ such as derived from thermal attachment experiments, see Fig. 3 and text).

ters $c_1 = 1.92$, 0.69, 0.13, and 0.05 at $T_{gas} = 300$, 400, 500, and 600 K respectively were derived for the SF_6-system [7].

4. Prediction of attachment cross sections and specific rate constants for autodetachment

After experimental attachment rate coefficients $k_{at}(T_{el}, T_{gas})$ have been analyzed in Section 3, we make use of the derived parameters and model the corresponding attachment cross sections

$$\sigma_{at}(E_{el}) = \left(\frac{\pi\hbar^2}{2\mu E_{el}}\right) \sum_{l=0}^{\infty} \sum_{m=-l}^{l} P_{l,m}^{VW}(\kappa) P_{l,m}^{IVR}(\kappa) \tag{4.1}$$

We show σ_{at} in Fig. 4, including partial waves up to $l = 2$ and employing the calculated capture probabilities $P_{l,m}^{VW}(\kappa)$ from Appendix A as well as the fitted IVR factors $P_{l,m}^{IVR}(\kappa)$ described in Section 3. The latter are consistent with the experimental attachment rate coefficients as a function of T_{el} (and, in this case, apparently do not show an additional dependence on T_{gas}). Fig. 4 also illustrates where the respective partial waves start to contribute to the cross sections.

For further kinetic modelling of the system, such as performed in part III [11], it is important to investigate whether the reverse of the attachment process, i.e. electron autodetachment, could compete with the dissociation of vibrationally excited $POCl_3^-$. The latter makes the reaction a dissociative electron attachment (DEA) process. Employing statistical unimolecular rate theory, analogous to the treatment of SF_6 in Ref. [7], we calculate specific rate constants $k_{det}(E, J)$ for electron detachment in the form

$$k_{det}(E, J) = \frac{W_{det}(E, J)}{h\rho(E, J)} \tag{4.2}$$

Here $\rho(E, J)$ denotes the rovibrational density of states of $POCl_3^-$ and $W_{det}(E, J)$ is the cumulative reaction probability as given by

$$W_{det}(E, J) = \sum_i P(E - E_{0i}) \tag{4.3}$$

The summation extends over all rovibrational states E_{0i} of neutral $POCl_3$ with $E_{0i} < E$. The internal energy E of $POCl_3^-$ is counted from the ground vibrational level of $POCl_3^-$. The $P(E - E_{0i})$ correspond to the attachment probabilities of Section 3 with κ replaced by $\kappa_i = \mu e[2\alpha(E - E_{0i})]^{1/2}/\hbar^2$. s-Wave and higher partial wave contributions are to be included. Further details of the procedure are described in Ref. [7]. The molecular parameters required for the calculations are summarized in Appendix B. The resulting specific rate constants $k_{det}(E, J = 0)$ for autodetachment are shown in Fig. 5. It turns out [11] that they are much smaller than the specific rate constants for dissociation of $POCl_3^-$ to $POCl_2^-$ + Cl such that autodetachment for this system can safely be neglected.

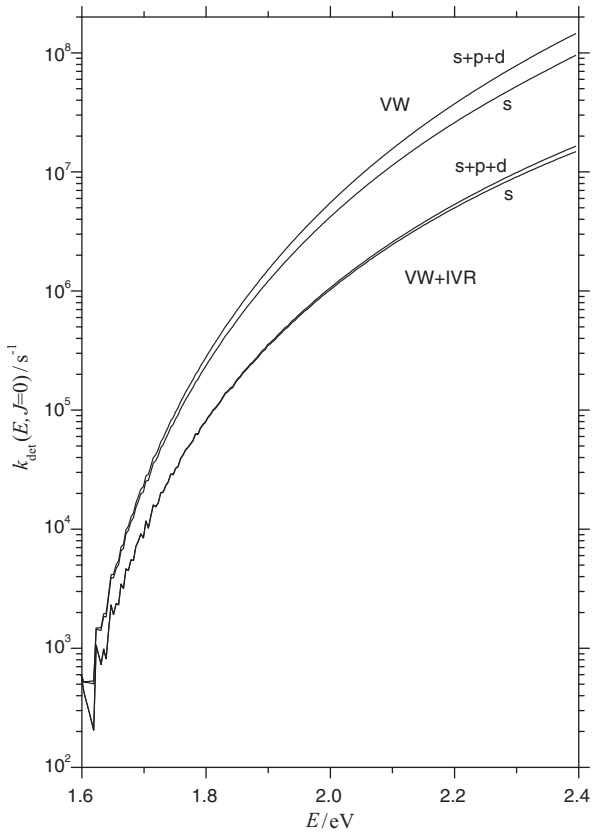

Fig. 5. Specific rate constants $k_{det}(E, J = 0)$ for detachment of electrons from $POCl_3^-$ (E = vibrational energy of $POCl_3^-$ counted from the vibrational zeropoint level; IVR factors with $(c_1, c_2) = (9, 0.03)$ such as derived from thermal attachment experiments, see Fig. 3 and text; upper curves: all-wave results and lower curves: s-wave results).

5. Conclusions

The measurement of DEA rate coefficients in the $POCl_3$ system over wide ranges of electron and bath gas temperatures has provided the opportunity to perform an analysis in terms of electron capture theory and to express the differences from experiments in terms of empirical IVR factors. A comparison of results for the polar $POCl_3$ target and the unpolar target SF_6 was made. It was shown that not only s-waves but also higher partial waves might have to be considered. The functional form of the derived IVR factors $P_s^{IVR}(\kappa)$ was similar to those tentatively assumed for SF_6. Being of similar magnitude as in SF_6^-, nevertheless quantitative differences of the dominant s-wave fit parameter c_1 were noted. The observed absence of a dependence of c_1 on T_{gas} also differs from the results for SF_6. It appears valuable now to have empirical IVR factors for the polar $POCl_3$ in comparison to the unpolar SF_6. Obviously the derived IVR factors wait for an interpretation in terms of rigorous attachment theory.

The analysis of experimental attachment rate coefficients as separate functions of gas and electron temperature has allowed us to predict cross sections as well as the specific rate constants for autodetachment of electrons from $POCl_3^-$. The comparison of the latter with specific rate constants for dissociation of vibrationally highly excited $POCl_3^-$, which will be considered in part III [11],

indicates that autodetachment does not play a role in this system, which differs from attachment experiments with SF_6 [7,9] and C_{60} [23,27]. The derived cross sections are an indispensible element for the analysis of the pressure and temperature dependences of the DEA product branching fractions analyzed in part III of this series [11].

Acknowledgments

This article is dedicated to Prof. Tino Gäumann from the Institut de Chimie-Physique of the Ecole Polytechnique Fédérale de Lausanne at the occasion of his 80th birthday. J.T. thanks him for life-long support and encouragement. Numerous discussions of this work with E.E. Nikitin and help by I. Litvin (Appendix A) and A. Maergoiz are gratefully acknowledged. The project was funded by the United States Air Force Office of Scientific Research under Project 2303EP. Financial support by the European Office of Aerospace Research and Development (Grant Award No. FA8655-10-1-3057) is also gratefully acknowledged. T.M.M. is under contract (FA8718-10-C-0002) from the Institute for Scientific Research of Boston College.

Appendix A.

Partial wave-selected electron capture probabilities $P^{VW}_{0,0}(\kappa, d=1)$ within the extended Vogt–Wannier capture model of Refs. [4,5,20,24].

For s-waves and a reduced dipole moment $d = e\mu\mu_D/\hbar^2 = 1.0$, the numerical results of Ref. [4] can well be approximated by

$$P^{VW}_{0,0}(\kappa,\ d=1) = 1 - 0.120\exp[-1.677(0.988+\log\kappa)^2] \qquad (A1.1)$$

For higher partial waves, the $P_{l,m}(\kappa, d=1)$ can be approximated by

$$P_{l,m}(\kappa,\ d) = \left(\frac{1}{\{1+\exp[-2H_{l,m}(\kappa,\ d)]\}}\right) \qquad (A1.2)$$

with

$$H_{l,m}(\kappa,\ d) = a_1[\kappa - \kappa^{1/2}_{l,m}(d)] + b_1[\kappa - \kappa^{1/2}_{l,m}(d)]^2 + c_1[\kappa - \kappa^{1/2}_{l,m}(d)]^3 \qquad (A1.3)$$

For $d=1$, the $\kappa^{1/2}_{l,m}$ $(d=1)$ are given as 1.31, 1.13, 3.21, 3.26, and 3.16 when $(l,m)=(1,0)$, $(1, |1|)$, $(2,0)$, $(2, |1|)$, and $(2, |2|)$, respectively. For further details, see Refs. [20,24]. The d-independent coefficients a_l, b_l, and c_l are [20,24] $(a_l,b_l,c_l)=(1.5,-0.5,0.1)$ and $(0.89,-0.138,0.018)$ for $l=1$, and 2, respectively.

Appendix B.

Molecular parameters for autodetachment calculations

Vibrational frequencies (in cm^{-1}). $POCl_3$: 1321.5, 480.5, 265.5, 590(2), 333(2), 187(2) from Ref. [25]. Our B3LYP/6-311+G(3df) calculations without scaling factor gave 1318.9, 461.4, 258.9, 567.3(2), 325.6(2), 183.1.

$POCl_3^-$: our B3LYP/6-311+G(3df) calculations gave 1245.8, 271.6, 135.1, 387.5, 405.6, 174.8, 210.5, 81.6, 40.1.

Rotational constants in (cm^{-1}). $POCl_3$: $A=B=0.0658$, $C=0.0478$; $\sigma=3$.

$POCl_3^-$: $A=0.0629$, $B=0.0459$, $C=0.0342$; $\sigma=1$.

Electron affinity of $POCl_3$: 1.41(±0.20) eV, experimental value from Ref. [26]; our G3 calculations gave 1.59(±0.1) eV.

References

[1] I.I. Fabrikant, H. Hotop, J. Chem. Phys. 128 (2008) 124308.
[2] H. Hotop, M.-W. Ruf, M. Allan, I.I. Fabrikant, Adv. At. Mol. Opt. Phys. 49 (2003) 85.
[3] I.I. Fabrikant, H. Hotop, Phys. Rev. A: At. Mol. Opt. Phys. 63 (2001) 022706.
[4] E.I. Dashevskaya, I. Litvin, E.E. Nikitin, J. Troe, Phys. Chem. Chem. Phys. 10 (2008) 1270.
[5] E.I. Dashevskaya, I. Litvin, E.E. Nikitin, J. Troe, J. Phys. Chem. A 113 (2009) 14212.
[6] E.E. Nikitin, J. Troe, Phys. Chem. Chem. Phys. 12 (2010) 9011.
[7] J. Troe, T.M. Miller, A.A. Viggiano, J. Chem. Phys. 127 (2007) 244303.
[8] I.I. Fabrikant, Phys. Rev. A 43 (1991) 3478.
[9] J. Troe, T.M. Miller, A.A. Viggiano, J. Chem. Phys. 127 (2007) 244304.
[10] J.M. Van Doren, J.F. Friedman, T.M. Miller, A.A. Viggiano, S. Denifl, P. Scheier, T.D. Märk, J. Troe, J. Chem. Phys. 124 (2006) 124322, part I of this series.
[11] T.M. Miller, N.S. Shuman, A.A. Viggiano, J. Troe, in preparation, part III of this series.
[12] T.M. Miller, J.V. Seeley, W.B. Knighton, R.F. Meads, A.A. Viggiano, R.A. Morris, J.M. Van Doren, J. Gu, H.F. Schaefer III, J. Chem. Phys. 109 (1998) 578.
[13] J.F. Friedman, T.M. Miller, J.K. Friedman-Schaffer, A.A. Viggiano, G.K. Rekha, A.E. Stevens, J. Chem. Phys. 128 (2008) 104303.
[14] T.M. Miller, Adv. At. Mol. Opt. Phys. 51 (2005) 299.
[15] T.M. Miller, J.F. Friedman, J.S. Williamson, L.C. Schaffer, A.A. Viggiano, Rev. Sci. Instrum. 80 (2009) 034104.
[16] D. Smith, P. Španěl, Adv. At. Mol. Opt. Phys. 32 (1994) 307–343.
[17] P. Španěl, Int. J. Mass Spectrom. Ion Process. 149/150 (1995) 299.
[18] T.M. Miller, J.F. Friedman, C.M. Caples, J.M. Van Doren, M.F. Bardaro Jr., P. Nguyen, C. Magee, A.A. Viggiano, J. Chem. Phys. 132 (2010) 214302.
[19] R.W. Crompton, G.N. Haddad, Australian J. Phys. 36 (1983) 15.
[20] E.I. Dashevskaya, I. Litvin, E.E. Nikitin, J. Troe, in preparation.
[21] R. Bosque, J. Sales, J. Chem. Inf. Comput. Sci. 42 (2002) 1154.
[22] D.R. Lide (Ed.), CRC Handbook of Chemistry and Physics, 88th ed., 2007/2008, Boca Raton.
[23] A.A. Viggiano, J.F. Friedman, N.S. Shuman, T.M. Miller, L.C. Schaffer, J. Troe, J. Chem. Phys. 132 (2010) 194307.
[24] E.E. Nikitin, J. Troe, Phys. Chem. Chem. Phys., in preparation.
[25] T. Shimanouchi, J. Phys. Chem. Ref. Data 6 (3) (1972) 993.
[26] B.P. Mathur, E.W. Rothe, S.Y. Tang, G. Reck, J. Chem. Phys. 64 (1976) 565.
[27] M. Lezius, Int. J. Mass Spectrom. 223/224 (2003) 447.